THE JOURNAL OF BIOLOGICAL CHEMISTRY VOL. 288, NO. 5, pp. 2952–2963, February 1, 2013


# Hyperactivation of the Mammalian Degenerin MDEG Promotes Caspase-8 Activation and Apoptosis*◆

Received for publication, November 29, 2012 Published, JBC Papers in Press, December 13, 2012, DOI 10.1074/jbc.M112.441063

**Ji-An Pan[‡], Yongjun Fan[‡], Rajesh Kumar Gandhirajan[§¶], Muniswamy Madesh[§¶], and Wei-Xing Zong[‡1]**

*From the [‡]Department of Molecular Genetics and Microbiology, Stony Brook University, Stony Brook, New York 11794 and the [§]Department of Biochemistry and [¶]Center for Translational Medicine, Temple University, Philadelphia, Pennsylvania 19140*

**Background:** Hyperactivation of DEG/ENaC channels leads to cell death; however, the underlying mechanism for the cytotoxicity remains unclear.
**Results:** A hyperactivation mutant MDEG G430F induces intracellular calcium rise, elevated ROS generation, inhibition of protein degradation, and intracellular caspase-8 aggregation and activation.
**Conclusion:** DEG/ENaC hyperactivation leads to a caspase-8-mediated apoptosis.
**Significance:** This study provides a novel mechanism for DEG/ENaC hyperactivation-mediated cytotoxicity.

**Intracellular calcium overload plays a critical role in numerous pathological syndromes such as heart failure, brain ischemia, and stroke. Hyperactivation of the acid-sensing ion channels including degenerin/epithelial amiloride-sensitive sodium (DEG/ENaC) channels has been shown to elevate intracellular calcium and cause subsequent neuronal cell death that is independent of the canonical Egl-1/Ced-9/Ced-4/Ced-3 apoptotic pathway in *Caenorhabditis elegans*. In mammalian cells, hyperactivation of the DEG/ENaC channels can also lead to cell death, although the underlying mechanism remains largely unknown. Here, we use a tetracycline-inducible system to express the hyperactivation mutant of a mammalian DEG/ENaC channel protein, MDEG G430F, in murine kidney epithelial cells deficient in the key mitochondrial apoptotic proteins Bax and Bak. Remarkably, expression of MDEG G430F induces increased intracellular calcium, reactive oxygen species (ROS) production, and cell death. The MDEG G430F-induced cell death is blocked by the intracellular calcium chelator 1,2-bis(*o*-aminophenoxy)ethane-*N*,*N*,*N*′,*N*′-tetraacetic acid (acetoxymethyl ester), ROS scavengers, and the caspase inhibitor z-VAD-fmk (where z and fmk are benzyloxycarbonyl and fluoromethyl ketone). Mechanistically, the intracellular calcium overload and ROS increase lead to the inhibition of proteasomal and autophagic protein degradation, which promotes the accumulation of protein aggregates containing caspase-8 and subsequent caspase-8 activation. As protein aggregation upon the inhibition of proteasomal and autophagic degradation pathways is mediated by the ubiquitin-binding protein SQSTM1/p62 and the autophagy-related protein LC3, silencing of p62 and LC3 protects cells from MDEG G430F-induced cell death. Our results uncover a new mechanism of caspase-8-mediated apoptosis induced by intracellular calcium overload that is dependent on the autophagy-related proteins LC3 and p62 upon hyperactivation of DEG/ENaC channels.**

The degenerin/epithelial sodium channels (DEG/ENaC)[2] are a family of amiloride-sensitive cell surface channels that allow apical entry of cations including $Na^+$ and $Li^+$ into cells. Some of these channels are nonselective and are permeable to larger ions such as $K^+$ and $Ca^{2+}$. A subset of these channels is activated by extracellular protons and is hence termed acid-sensing ion channels. Proper function of these channels is critical for maintaining cellular ion homeostasis and osmotic balance. Although previously thought to be mostly expressed in fluid absorptive epithelia and in neurons, these channels have since been found to be expressed in most tissues (1, 2). Dysregulation of DEG/ENaC channels has been implicated in numerous pathological conditions ranging from hypertension, anxiety disorder, and neurodegenerative disorder to cancer, many of which are associated with hyperactivation-induced cytotoxicity. Modulation of DEG/ENaC channel activity has become an emerging therapeutic opportunity (2–4).

The cytotoxicity of DEG/ENaC hyperactivation was initially recognized in *Caenorhabditis elegans*. The gain-of-function mutants of DEG-1, MEC-4, and MEC-10 led to necrosis-like cell death in *C. elegans* sensory neurons (5, 6). It has been suggested that the rise in intracellular $Ca^{2+}$ induced by the gain-of-function mutants of the DEG/ENaC channels is the cause for cell death (7–9). This DEG/ENaC hyperactivation-induced cell death in *C. elegans* is independent of the canonical apoptosis regulators EGL-1, CED-9, and CED-3, but rather is mediated by the $Ca^{2+}$-dependent activation of calpain and aspartyl proteases (10).

The mammalian degenerin homolog (MDEG) was originally cloned from human and rat brains (11). Similar to the gain-of-function DEG-1(d), MEC-4(d), and MEC-10(d) mutants in

* This work was supported, in whole or in part, by National Institutes of Health Grants CA129536 and GM097355 (to W. X. Z) and HL086699 (to M. M.).
◆ This article was selected as a Paper of the Week.
[1] To whom correspondence should be addressed. Tel.: 631-632-4104; Fax: 631-632-9797; E-mail: wzong@notes.cc.sunysb.edu.

[2] The abbreviations used are: DEG/ENaC, degenerin/epithelial sodium channels; MDEG, mammalian degenerin homolog; ROS, reactive oxygen species; BAPTA-AM, 1,2-bis(*o*-aminophenoxy)ethane-*N*,*N*,*N*′,*N*′-tetraacetic acid (acetoxymethyl ester); 3-MA, 3-methyladenine; LC3, light chain 3; TEMPOL, 4-hydroxy-TEMPO; Tiron, 4,5-dihydroxy-1,3-benzenedisulfonic acid disodium salt monohydrate; DOX, doxycycline hyclate; PI, propidium iodide; z, benzyloxycarbonyl; CM-$H_2$DCFDA, 5-(and-6) chloromethyl-2′,7′ dichlorodihydrofluorescein diacetate acetyl ester; fmk, fluoromethyl ketone; PARP, poly(ADP-ribose) polymerase; Ub, ubiquitin; BMK, baby mouse kidney; WB, Western blot.

*C. elegans*, the substitution of glycine 430 in MDEG with an amino acid bulkier than serine such as phenylalanine leads to its constitutive activation. Ectopic expression of the MDEG G430F mutant led to cell death in *Xenopus* oocytes, human kidney cell line HEK293, and *C. elegans* sensory neurons (11). However, the molecular mechanism underlying this MDEG G430F-induced cell death in mammalian cells remains unknown. In the present study, we provide evidence that MDEG G430F triggers protein aggregation-mediated caspase-8 activation and apoptosis.

## EXPERIMENTAL PROCEDURES

*Cell Lines, Culture, and Transfection*—HEK293T and $bax^{-/-}$ $bak^{-/-}$ baby mouse kidney (BMK) cells were cultured in Dulbecco's modified Eagle's medium (DMEM) supplemented with 10% FBS, 100 units/ml penicillin, and 100 μg/ml streptomycin (Invitrogen). Lipofectamine 2000 (Invitrogen) was used for transfection. Rat MDEG and MDEG (G430F) expression constructs were a gift from Dr. Michel Lazdunski (11). MDEG and MDEG (G430F) sequences were amplified by PCR with primers (5′-AGTCGACATGGACCTCAAGGAGAGCCCCAGTGAG-3′ and 5′-AATCGATTTAGTGATGATGGTGGTGATGCTCGCAGGCAATCTCCTCCAGGGTGC-3′) and were inserted into the pRev-TRE vector. cDNA sequences with MDEG and MDEG G430F fused with GFP at their C terminus were also inserted into the pRev-TRE vector. The retrovirus encoding rtTA2-M2 activator, TRSID silencer, and puromycin selection marker (pLIB-rtTAM2iresTRSIDiresPuro, a gift from Dr. M. Ausserlechner of Medical University Innsbruck, Austria) (12) and the pRev-TRE retrovirus encoding MDEG, MDEG (G430F), MDEG-GFP, or MDEG (G430F)-GFP were used to co-infect cells. The infected cells were selected by puromycin (2 μg/ml) and hygromycin (2 mg/ml). Single cell clones were selected. shRNAs were purchased from Sigma (for LC3, NM_025735, CATGAGCGAGTTGGTCAAGAT; for p62, NM_011018, CCGCATCTACATTAAAGAGAA; for caspase-8, NM_009812, CCTCCATCTATGACCTGACA).

*Reagents and Antibodies*—The following reagents were used: z-VAD-fmk (Calbiochem 219007), Hoechst 33342 (Molecular Probes H1399, used at 0.5 μg/ml), 4′,6-diamidino-2-phenylindole dihydrochloride (DAPI) (Sigma D9542, used at 1 μg/ml), 3-methyladenine (3-MA) (Sigma 08592, used at 5 mM), chloroquine (Sigma C6628, used at 10 μM), nickel-nitrilotriacetic acid-agarose (Qiagen 133203974), Tiron (Fluka 89460, used at 5 mM), BAPTA (Sigma A4926), BAPTA-AM (Sigma A1076, used at 30 μM), EGTA (Sigma E3889), 4-hydroxy-TEMPO (TEMPOL) (Sigma 176141, used at 5 mM), amiloride (Sigma A7410, used at 800 μM), CM-$H_2$DCFDA (Invitrogen C6827, used at 10 μM), doxycycline hyclate (DOX) (Sigma D9891, used at 0.5 μg/ml), bafilomycin A1 (used at 50 nM), Dual-Luciferase reporter assay system (Promega E1910), and propidium iodide (PI) (Invitrogen P3566, used at 1 μg/ml for cell death assay).

The following antibodies were used: poly(ADP-ribose) polymerase (PARP) (Cell Signaling Technology 9542, 1:1,000 for WB), caspase-8 (R&D Systems AF1650, 1:1,000 for WB; Alexis Biochemicals Alx-804-447, 1:200 for immunofluorescence), caspase-3 (Cell Signaling Technology 9661, 1:1,000 for WB), tubulin (Sigma T4026, 1:10,000 for WB), p62 (Abnova H00008878-M01, clone 2C11, 1: 5,000 for WB), GFP (Santa Cruz Biotechnology sc-9996, 1:1,000 for WB, 1 μg/reaction for immunoprecipitation), rabbit GFP antibody (a gift from Dr. Zhenyu Yue, Mount Sinai School of Medicine, 1:2,000 for WB, 0.3 μg/reaction for immunoprecipitation), and LC3 (MBL International PM036, 1:1,000 for WB).

*Lentiviral and Retroviral Infection*—For lentiviral infection, HEK293T cells ($5 \times 10^5$) were plated into a 3-cm culture dish. After overnight recovery, cells were transfected with the viral packaging plasmid pCMV Δ8.91 (2 μg), a vesicular stomatitis virus glycoprotein expression plasmid (1 μg), and the lentiviral expression plasmid (3 μg) using Lipofectamine 2000. The medium was replaced with fresh medium 4 h after transfection. 20 h later, the virus-containing cell culture supernatant was filtered through a 0.45-μm nylon filter and subsequently used to infect $bax^{-/-}bak^{-/-}$ BMK cells. The infection procedure was repeated two more times every 12 h. 24 h after the last infection, cells were selected with 2 μg/ml puromycin. Retroviral infection was performed as described previously (13). Briefly, retrovirus was produced in HEK293T cells after transfection with LPC retroviral constructs (2.5 μg) and helper viral construct (1.5 μg). The same infection procedure as lentiviral infection was used, except that the viral supernatant was supplemented with 10 μg/ml Polybrene (Sigma).

*His-Ub Assay for Mammalian Cells*—$3 \times 10^6$ cells were plated into a 10-cm culture dish. After overnight recovery, cells were transfected with 2 μg of pMT107 plasmid encoding polyhistidine-tagged Ub. 1 day after transfection, cells were collected, and the same number of cells was plated into multiple wells for treatment. After treatment, cells were collected, washed twice with phosphate-buffered saline (PBS), and resuspended in 1 ml of buffer A (6 M guanidine-HCl, 0.1 M $Na_2HPO_4$/$NaH_2PO_4$, 10 mM imidazole, pH 8.0). After 10 s of sonication, 50 μl of nickel-nitrilotriacetic acid-agarose (Qiagen) equilibrated with buffer A was added to each sample and incubated for 3 h at room temperature with agitation. Agarose was precipitated by centrifugation and washed twice with buffer B (10 mM Tris-Cl, pH 8.0, 8 M urea, 0.1 M $NaH_2PO_4$) and three times with 1:4 diluted buffer B. The precipitates were resuspended in 100 μl of 2× Laemmli buffer (4% SDS, 20% glycerol, 10% 2-mercaptoethanol, 0.004% bromphenol blue, 0.125 M Tris-HCl, pH 6.8) with 200 mM imidazole, heated at 95 °C for 10 min, and subjected to Western blotting.

*Measurement of Proteasome Activity*—$2 \times 10^4$ cells were plated into a 24-well plate. The ubiquitin-luciferase bioluminescence imaging reporter (Ub-FL) (14) and *Renilla* luciferase control plasmids were transfected into cells, and medium was replaced with fresh medium 5 h later. 16 h after transfection, the transfected cells were left untreated or treated with DOX or other indicated combinations. 24 h after treatment, the luciferase activities were measured by the Dual-Luciferase reporter assay system.

*Detection of Intracellular ROS*—$5 \times 10^5$ cells were plated into 6-cm dishes. After overnight recovery, cells were untreated or treated with DOX together with other agents. 24 h after treatment, cells were incubated with CM-$H_2$DCFDA (10 μM final concentration) for 30 min in the dark and collected. The collected cells were resuspended in DMEM without phenol red

and analyzed with a flow cytometer using the CellQuest program.

*Caspase-8 Activity Assay*—Caspase-8 activity was determined using the Caspase-Glo 8 assay kit (Promega G8200), which uses the luminogenic caspase substrate, following the manufacturer's instructions. Luciferase activities were read by a luminescence reader (SpectraMax M5, Molecular Devices).

*Measurement of Cell Death*—For cell viability, two methods were used. For PI exclusion assay, cells (including the detached ones) were collected and resuspended in culture medium with PI at 1 $\mu$g/ml. Cell viability was determined by flow cytometry using a FACSCalibur. For trypan blue staining, 0.5 ml of cells (around $1 \times 10^5$ cells/ml) was mixed with 0.1 ml of 0.4% trypan blue and incubated for 5 min at room temperature. Cells were counted under a phase contrast light microscope.

*Calcium Imaging and Quantification*—MDEG G430F was treated with DOX (0.5 $\mu$g/ml). To perform time-course experiments, cells expressing wild-type MDEG and MDEG G430F were cultured on 25-mm diameter glass coverslips in 6-well plates, and cells were loaded with the cytosolic $Ca^{2+}$ indicator Fluo-4/AM (Invitrogen, 5 $\mu$M;) at room temperature for 30 min in extracellular medium containing 121 mM NaCl, 5 mM $NaHCO_3$, 10 mM Na-HEPES, 4.7 mM KCl, 1.2 mM $KH_2PO_4$, 1.2 mM $MgSO_4$, 2 mM $CaCl_2$, 10 mM glucose, and 2.0% bovine serum albumin (BSA), pH 7.4, in the presence of 100 $\mu$M sulfinpyrazone and 0.003% pluronic acid. After dye loading, cells were washed and resuspended in the experimental imaging solution (extracellular medium containing 0.25% BSA), and images were acquired using the temperature-controlled Carl Zeiss LSM510 META confocal imaging system with 40×/1.3 NA oil objective. Cytosolic Fluo-4 changes were analyzed and quantified using ImageJ software (National Institutes of Health) as described previously (15).

*GFP-LC3 Puncta Observation and Quantification*—Quantification of GFP-LC3 puncta was performed as described previously (16). Briefly, cells stably expressing GFP-LC3 were fixed in 4% paraformaldehyde in PBS and observed under an inverted deconvolution microscope (Axiovert 200M; Carl Zeiss, Inc.) using the 63× oil objective lens. The cells with more than 10 obvious puncta were selected for quantification. ~100 cells were randomly selected and counted.

*Statistics*—Data from cell death assays are presented as mean ± S.D.

*Image Processing and Densitometry Measurement*—Images taken from deconvolution and confocal microscopes were viewed and processed by AxioVision LE and Zeiss LSM image browser, respectively. Images were processed in Adobe Photoshop to enhance the brightness and contrast. Densitometry of immunoblot bands was determined by ImageJ software, unless indicated otherwise.

## RESULTS

*Expression of MDEG G430F Leads to an Increase in Intracellular Calcium, ROS Generation, and Apoptosis*—Because MEC-4(d)-induced cell death is not inhibited by the Bcl-2 homolog Ced-9 (17), we reasoned that MDEG hyperactivation may also induce cell death independent of mitochondrial apoptosis in mammalian cells. Therefore, we used the BMK cells with genetic deletion of both Bax and Bak (18), the two key regulators of mitochondrial apoptosis (19–21).

GFP-tagged wild-type and the G430F mutant MDEG were constructed into a tetracycline-regulated expression system and stably transfected into $bax^{-/-}bak^{-/-}$ BMK cells. The addition of doxycycline induced progressive expression of MDEG proteins (Fig. 1*A*). As expected, MDEG was predominantly localized to the plasma membrane (Fig. 1*B*). We were unable to obtain a clear subcellular localization pattern for MDEG G430F due to the rapid induction of cell death (Fig. 1, *C* and *D*). Although cells expressing wild-type MDEG appeared normal, expression of MDEG G430F led to massive cell death after 48 h as indicated by cell morphology, nuclear fragmentation, and loss of plasma membrane integrity (Fig. 1, *C* and *D*). Furthermore, MDEG G430F-induced cell death is blocked by amiloride, the chemical inhibitor of ENaC (Fig. 1*E*), indicating that this cell death is specifically mediated by hyperactivation of MDEG.

Because hyperactivated MEC-4(d) mutant was reported to increase intracellular $Ca^{2+}$ (9), we assessed whether MDEG G430F could also induce intracellular calcium rise. Indeed, ectopic expression of MDEG G430F, but not wild-type MDEG, led to a significant increase in intracellular $Ca^{2+}$ levels (Fig. 2, *A* and *B*). Furthermore, the cell-permeable calcium chelator BAPTA-AM blocked cell death (Fig. 2*C*), whereas the cell-impermeable chelators BAPTA and EGTA did not (Fig. 2*D*), suggesting that the intracellular $Ca^{2+}$ rise is a result of endoplasmic reticulum $Ca^{2+}$ emptying. We went on to determine how cytoplasmic $Ca^{2+}$ overload promotes cell death. To this end, ROS production is considered a main molecular consequence of intracellular $Ca^{2+}$ rise (22). Indeed, MDEG G430F induced ROS production, which was inhibited by amiloride and the ROS scavenger TEMPOL (Fig. 2*E*). Importantly, BAPTA-AM also inhibited ROS production (Fig. 2*E*), indicating that the cytoplasmic $Ca^{2+}$ overload was responsible for the increased level of ROS. Furthermore, MDEG G430F-induced cell death was significantly inhibited by ROS scavengers Tiron and TEMPOL (Fig. 2*F*). These results indicate that hyperactivation of the amiloride-sensitive ENaC MDEG can lead to intracellular $Ca^{2+}$ rise, ROS overproduction, and cell death.

*MDEG G430F-mediated Apoptosis Is Mediated by Caspase-8*—Although the cell death induced by MDEG G430F occurs in Bax/Bak doubly deficient cells, the morphological appearance and nuclear fragmentation indicate that this cell death is still apoptotic (Fig. 1*C*). In agreement with this notion, the pan-caspase inhibitor z-VAD-fmk at least partially blocked cell death (Fig. 3*A*), indicating the involvement of caspase activation. Moreover, immunoblotting showed that the caspase cascade was activated by MDEG G430F expression, indicated by apoptotic cleavage of caspase-8, caspase-3, and PARP (Fig. 3*B*). The activation of caspase-8, an initiator caspase, accompanied by its cleavage, was determined using the Caspase-Glo 8 luminogenic assay kit (Fig. 3*C*). Consistent with the inhibition of apoptosis by amiloride, BAPTA-AM, ROS scavengers, and z-VAD-fmk (Figs. 1 and 2), these agents inhibited caspase-8 activation (Fig. 3*D*). To determine whether the activation of caspase-8 contributes to cell death induced by MDEG G430F, caspase-8 was knocked down using shRNA (Fig. 3*E*), which led

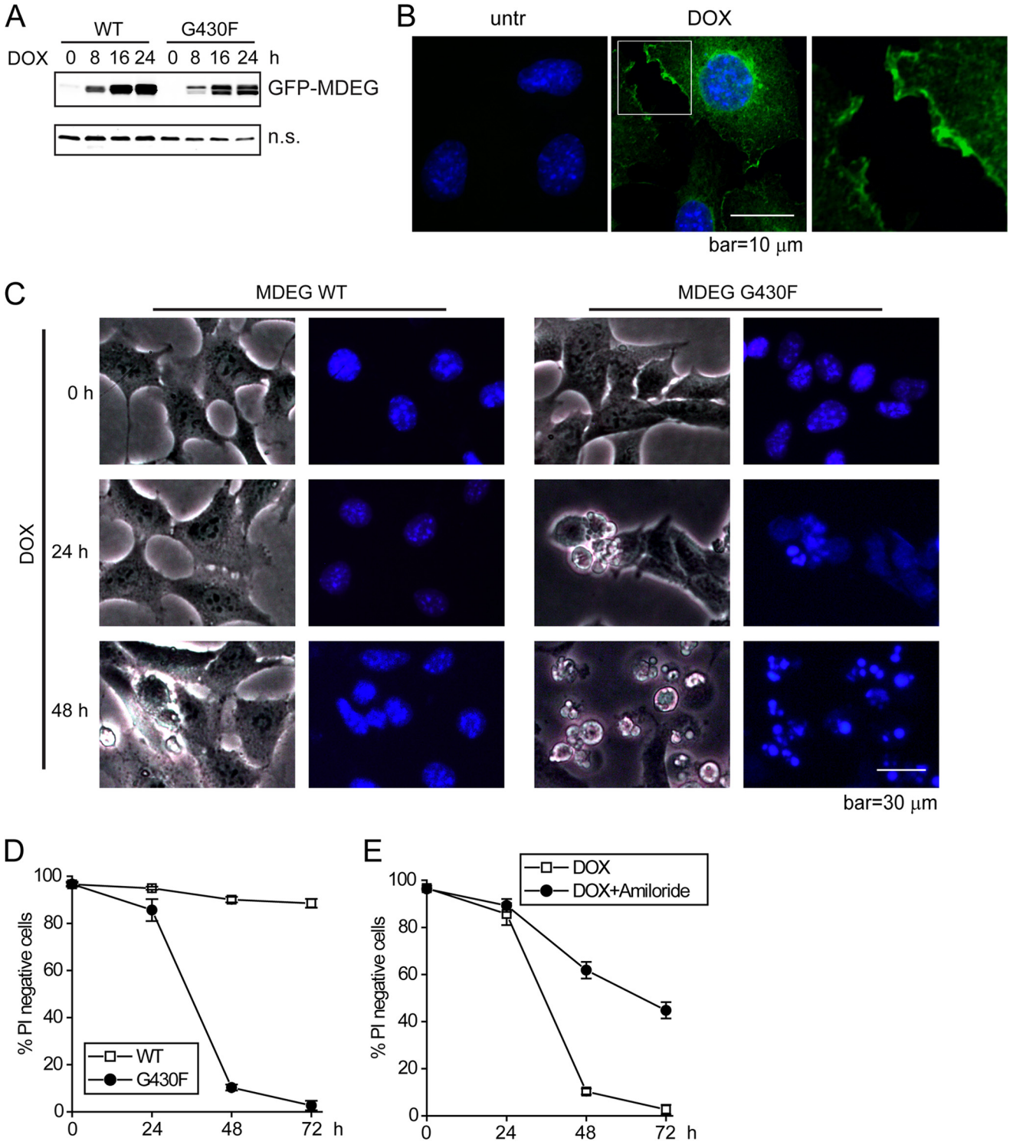


FIGURE 1. **MDEG G430F induces cell death in cells deficient in mitochondrial apoptosis.** *bax*$^{-/-}$*bak*$^{-/-}$ BMK cells with inducible expression of GFP-tagged wild-type MDEG and MDEG G430F were treated with DOX for the indicated times. *A*, expression of MDEG proteins was examined by Western blotting. A nonspecific band (*n.s.*) was used as a control for equal loading. *B*, MDEG-GFP expression after 16 h of DOX treatment was observed under a deconvolution microscope. Cells were stained with DAPI. Note the plasma membrane localization of MDEG, which is highlighted in a higher magnification view shown in the *right*. *untr*, untreated. *C*, cells were stained with the live cell-permeable dye Hoechst 33342 and observed and photographed under a fluorescence microscope. Representative images are shown. Note nuclear fragmentation in MDEG G430F cells. *D*, cell death was measured by PI exclusion. The average of three independent assays ± S.D. is shown. *E*, MDEG G430F cells were treated with DOX alone or together with amiloride. Cell death was measured by PI exclusion. The average of three independent assays ± S.D. is shown.

to a significant lower activity of caspase-8 (Fig. 3*F*) and conferred protection against MDEG G430F expression indicated by both PI exclusion and reduced cleavage of caspase-3 and PARP (Fig. 3, *G* and *H*). These data indicate that cell death induced by MDEG G430F is mediated by activation of caspase-8.

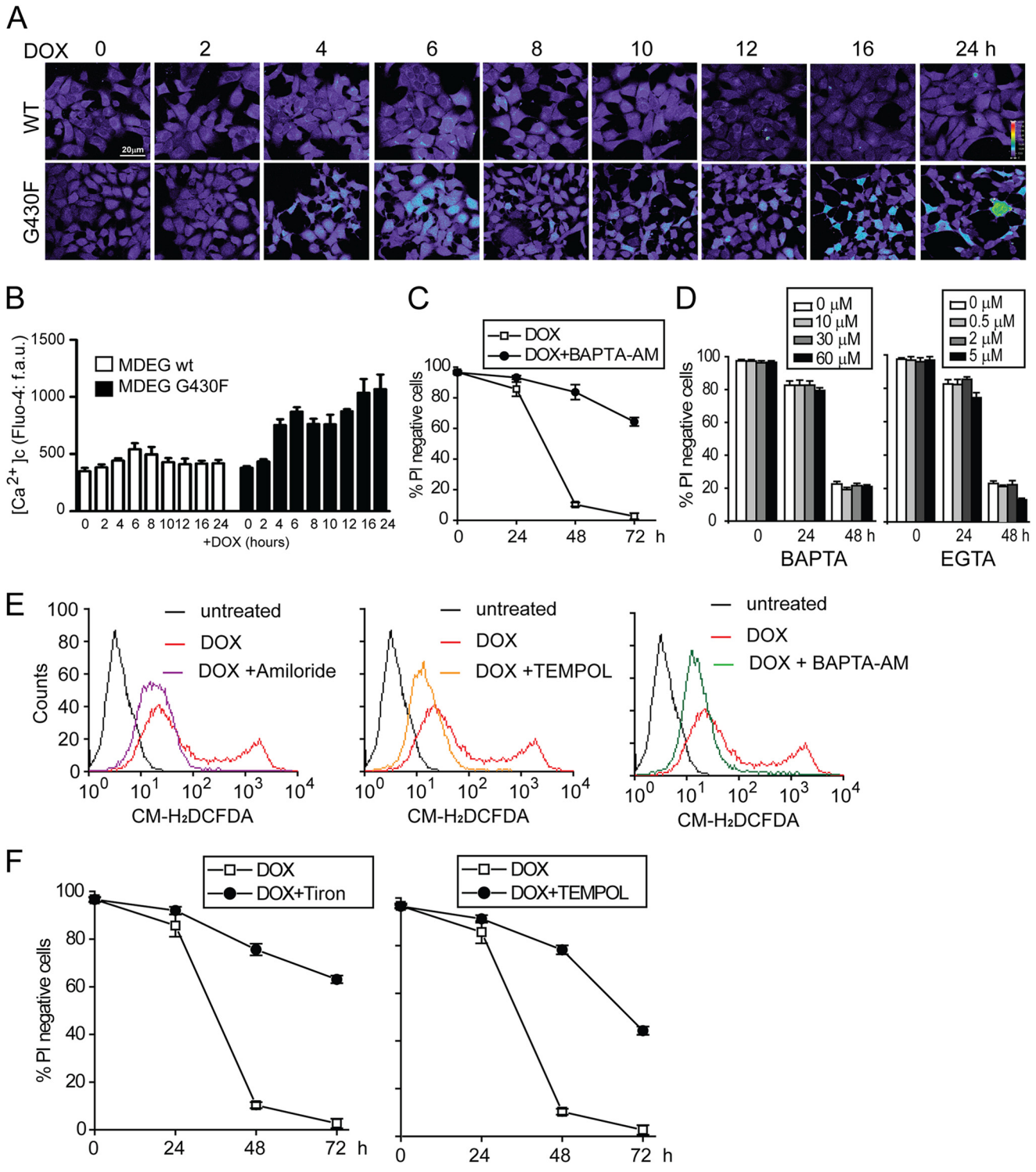


FIGURE 2. **MDEG G430F induces cell death via intracellular calcium rise and elevated ROS.** *A* and *B*, a time course of intracellular $Ca^{2+}$ in cells expressing wild-type MDEG or the MDEG G430F mutant following treatment with DOX. *A*, representative Fluo-4 fluorescence images were acquired using confocal microscopy at the indicated time points. *B*, quantification of Fluo-4 fluorescence intensity in *A* is expressed as fluorescence arbitrary unit (*f.a.u.*). Cumulative data are the mean ± S.D. of three independent experiments, each consisting of triplicate analyses of 20–40 cells. *C*, MDEG G430F-expressing cells were treated with DOX in the absence or presence of the cell-permeable calcium chelator BAPTA-AM. Cell death was measured by PI exclusion. The average of three independent assays ± S.D. is shown. *D*, MDEG G430F cells were treated with DOX alone or together with the cell-impermeable calcium chelators BAPTA or EGTA. Cell death was measured by PI exclusion. The average of three independent assays ± S.D. is shown. *E*, MDEG G430F cells were treated with DOX alone, or together with amiloride, BAPTA-AM, or TEMPOL. 24 h after treatment, cells were incubated with CM-$H_2$DCFDA for 30 min in the dark and then resuspended in DMEM without phenol red and analyzed by flow cytometry. Note increased ROS production upon DOX treatment, which is reduced in the presence of amiloride, BAPTA-AM, and TEMPOL. *F*, MDEG G430F cells were treated with DOX alone or in the presence of the ROS scavengers Tiron or TEMPOL. Cell death was measured by PI exclusion. The average of three independent assays ± S.D. is shown.

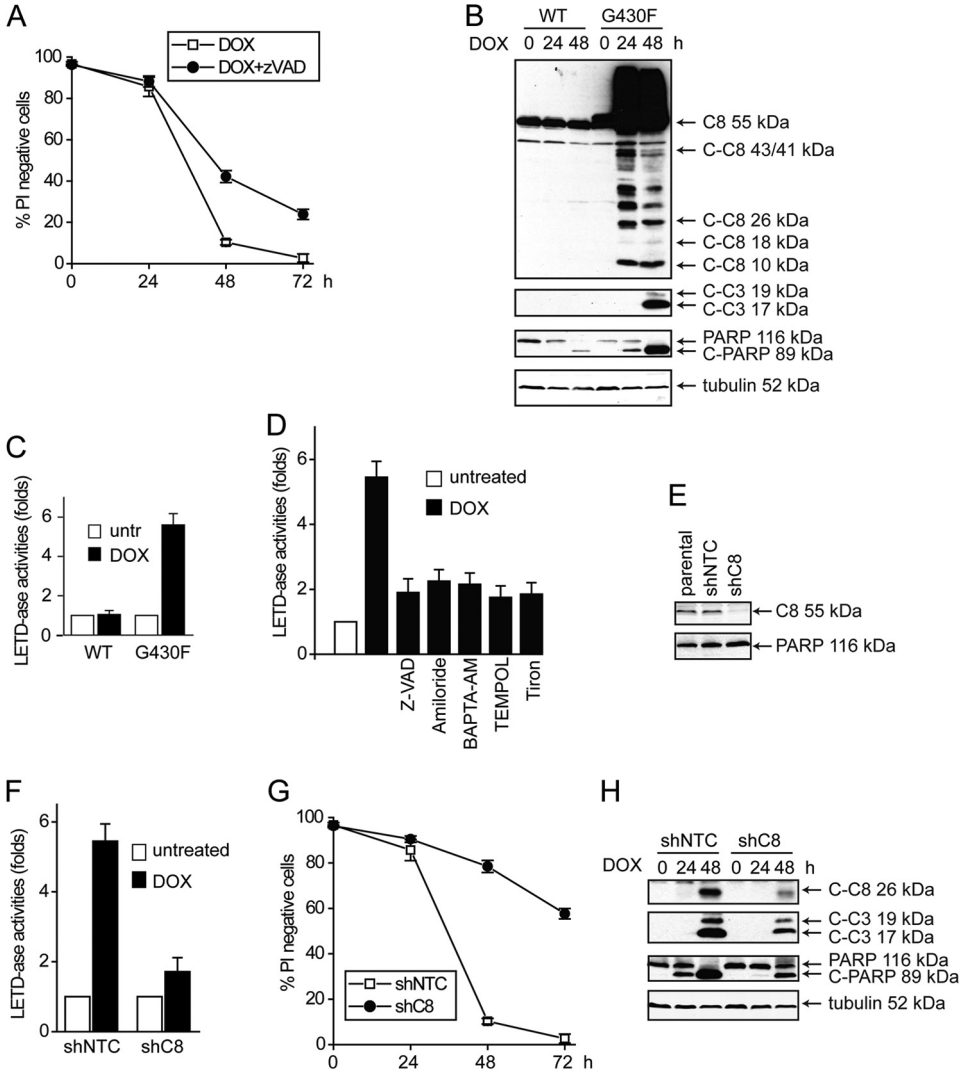


FIGURE 3. **MDEG G430F induces caspase-8-dependent apoptosis.** *A*, MDEG G430F cells were treated with DOX in the absence or presence of z-VAD-fmk. Cell death was measured by PI exclusion. The average of three independent assays ± S.D. is shown. *B*, cell lysates were collected at 24 and 48 h and examined by immunoblotting for the indicated proteins. *C-PARP*, cleaved PARP. *C*, cells expressing wild-type MDEG or MDEG G430F were treated with DOX for 24 h. Caspase-8 activity was assayed using Caspase-Glo 8 luminogenic assay kits. The average of three independent assays ± S.D. is shown. *untr*, untreated. *D*, MDEG G430F cells were treated with DOX alone or together with z-VAD-fmk, amiloride, BAPTA-AM, TEMPOL, or Tiron. 24 h later, caspase-8 activity was assayed using the Caspase-Glo 8 luminogenic kit. *E*, MDEG G430F cells were infected with lentiviral nontargeting control (*shNTC*) or caspase-8 (*shC8*) shRNAs. Knockdown of the caspase-8 was verified by immunoblotting. *F–H*, MDEG G430F cells infected with shNTC and shC8 shRNAs were treated with DOX. *F*, 24 h later, caspase-8 activity was determined. Cell death was measured by PI exclusion. *G*, the average of three independent assays ± S.D. is shown. *H*, cell lysates were collected and examined by immunoblotting for the indicated proteins.

*MDEG G430F Leads to Proteasome Inhibition and Accumulation of Polyubiquitinated Caspase-8*—We then went on to study how caspase-8 is activated upon hyperactivation of MDEG. We recently reported that caspase-8 can be activated, independently of death receptors, by the inhibition of intracellular protein degradation machineries (23, 24). Indeed, expression of MDEG G430F led to an accumulation of polyubiquitinated proteins (Fig. 4*B*), indicating an inhibition of intracellular protein degradation machineries. Intracellular calcium rise and ROS have been shown to inhibit proteasome activity (25–27). Because MDEG G430F could induce intracellular calcium rise (Fig. 2, *A* and *B*) and ROS generation (Fig. 2*D*), and amiloride, BAPTA-AM, and ROS scavengers could block caspase-8 activation (Fig. 3*G*), it is possible that MDEG G430F can lead to caspase-8 activation via proteasome inhibition. Indeed, increased levels of slow migrating caspase-8 species were observed in SDS-PAGE upon MDEG G430F expression (Fig. 3*B*). To determine whether MDEG G430F can lead to proteasome inhibition, we utilized a ubiquitin-luciferase reporter construct (14). This reporter construct is rapidly degraded by the 26 S proteasome, leading to low luciferase activity. Upon inhibition of proteasomal protein degradation, luciferase levels increase (14). Although wild-type MDEG did not alter proteasome activity, MDEG G430F expression led to strong proteasome inhibition (Fig. 4*A*). This proteasome inhibition was alleviated by amiloride, BAPTA-AM, TEMPOL, and Tiron (Fig. 4*A*), indicating that it was mediated by MDEG hyperactivation-induced intracellular calcium rise and ROS production. Consistent with proteasome inhibition shown by the luciferase reporter assay, MDEG G430F expression led to accumulation of polyubiquitinated proteins that was blocked by amiloride, BAPTA-AM, and TEMPOL, but not by z-VAD-fmk (Fig. 4*B*).

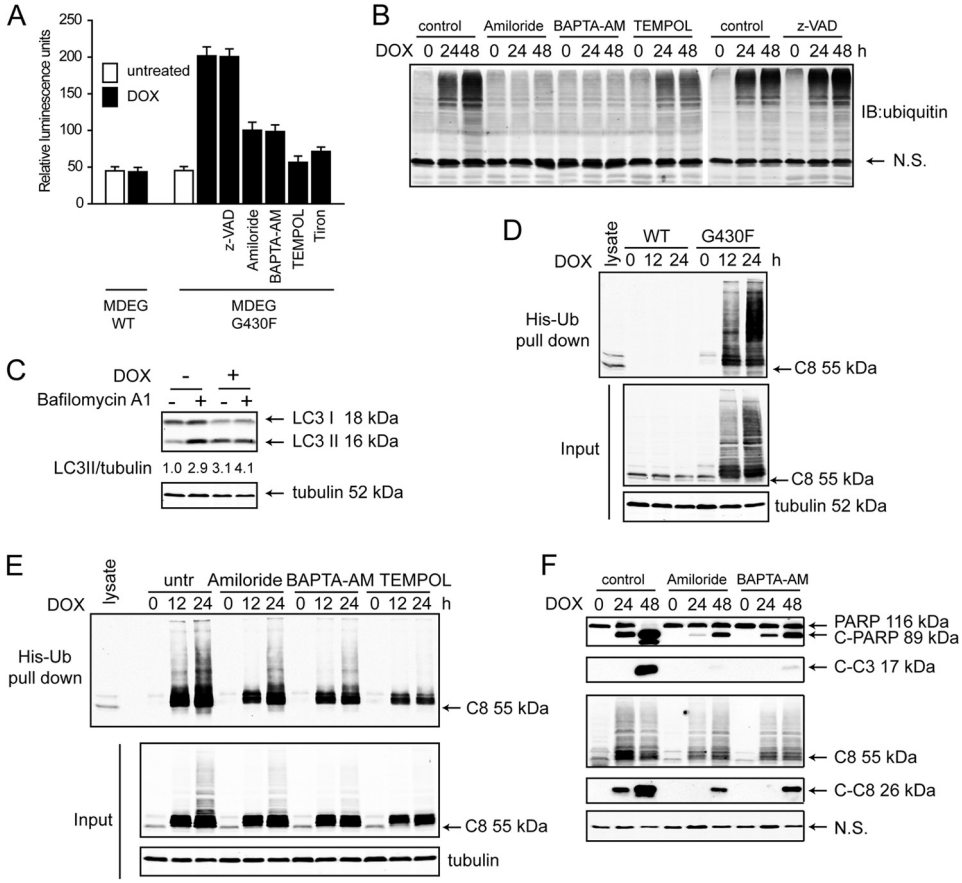


FIGURE 4. **MDEG G430F inhibits proteasomal degradation via increased intracellular $Ca^{2+}$ and ROS.** *A*, cells expressing wild-type MDEG or MDEG G430F were transfected with the ubiquitin-luciferase bioluminescence imaging reporter (Ub-FL) and the *Renilla* luciferase control plasmid. 24 h after transfection, cells were left untreated or treated with DOX alone or together with z-VAD-fmk, amiloride, BAPTA-AM, TEMPOL, or Tiron. 16 h later, luciferase activity in cell lysates was determined. Transfection efficiency was standardized against *Renilla* luciferase activity. The average of three independent assays ± S.D. is shown. *B*, MDEG G430F cells were treated with DOX alone, or together with amiloride, BAPTA-AM, TEMPOL, or z-VAD-fmk. Cell lysates were collected at various times, and the total ubiquitinated protein was examined by immunoblotting (*IB*). *N.S.*, nonspecific band. *C*, MDEG G430F cells cultured in the absence or presence of DOX were treated with the lysosomal inhibitor bafilomycin A1 for 12 h. Cell lysates were probed for LC3. The Western blot bands were quantified by densitometry. The ratio of LC3-II *versus* tubulin is shown. Note that in the absence of DOX, bafilomycin A1 leads to accumulation of LC3-II, indicating the basal level autophagy flux. LC3-II level is higher in the cells with DOX and is minimally increased upon bafilomycin A1 treatment, indicating a block of autophagy flux. *D*, cells expressing wild-type MDEG or MDEG G430F were transfected with His-Ub plasmid and then treated with DOX. Cell lysates were subjected to nickel-bead pulldown at the indicated times and examined by immunoblotting for the indicated proteins. *E*, after being transfected with His-Ub plasmid, MDEG G430F-expressing cells were treated with DOX alone or together with amiloride, BAPTA-AM, or TEMPOL. Cell lysates were subjected to nickel-bead pulldown at the indicated times and examined by immunoblotting for the indicated proteins. *untr*, untreated. *F*, MDEG G430F cells were treated with DOX alone or together with amiloride or BAPTA-AM. Cell lysates were collected and examined by immunoblotting for the indicated proteins.

Consistent with the literature showing that profound proteasomal inhibition can lead to the inhibition of the autophagolysosomal degradation (28, 29), MDEG G430F-expressing cells showed decreased autophagy flux indicated by reduced LC3 accumulation upon the treatment with the lysosomal inhibitor bafilomycin A1 (Fig. 4*C*).

To demonstrate that this MDEG G430F-induced inhibition of protein degradation can lead to an accumulation of polyubiquitinated caspase-8, His-tagged ubiquitin was transfected into cells expressing either wild-type MDEG or MDEG G430F. His pulldown was performed and showed increased caspase-8 ubiquitination only upon MDEG G430F expression (Fig. 4*D*), which was reduced by amiloride, BAPTA-AM, and TEMPOL (Fig. 4*E*). The amount of ubiquitinated caspase-8 correlated with apoptotic cleavage of caspase-8, caspase-3, and PARP (Fig. 4*F*). Together, these results indicate that MDEG G430F induces apoptosis by promoting proteasome inhibition and accumulation of ubiquitinated caspase-8.

*MDEG G430F Leads to Caspase-8 Aggregation and Association with LC3 and p62*—Inhibition of protein degradation has recently been shown to promote caspase-8 oligomerization via its interaction with p62 and LC3 (23, 24, 30). Proteasome inhibition leads to accumulation of protein aggregates that contain ubiquitinated caspase-8. The aggregates are recruited by the ubiquitin-binding protein SQSTM1/p62 and shuttled to autophagosomes for degradation via the interaction between p62 and the autophagy "receptor" protein LC3. As excessive proteasome inhibition also leads to the inhibition of autophagic degradation (31, 32), it eventually leads to the accumulation of protein aggregates that promotes caspase-8 oligomerization, activation, and apoptosis (24, 30).

Because we observed proteasome inhibition and accumulation of ubiquitinated caspase-8 upon MDEG G430F expression (Fig. 4), we went on to determine whether MDEG G430F can lead to caspase-8 association with LC3 and p62. Indeed, immunofluorescence showed that MDEG G430F expression induced large-sized

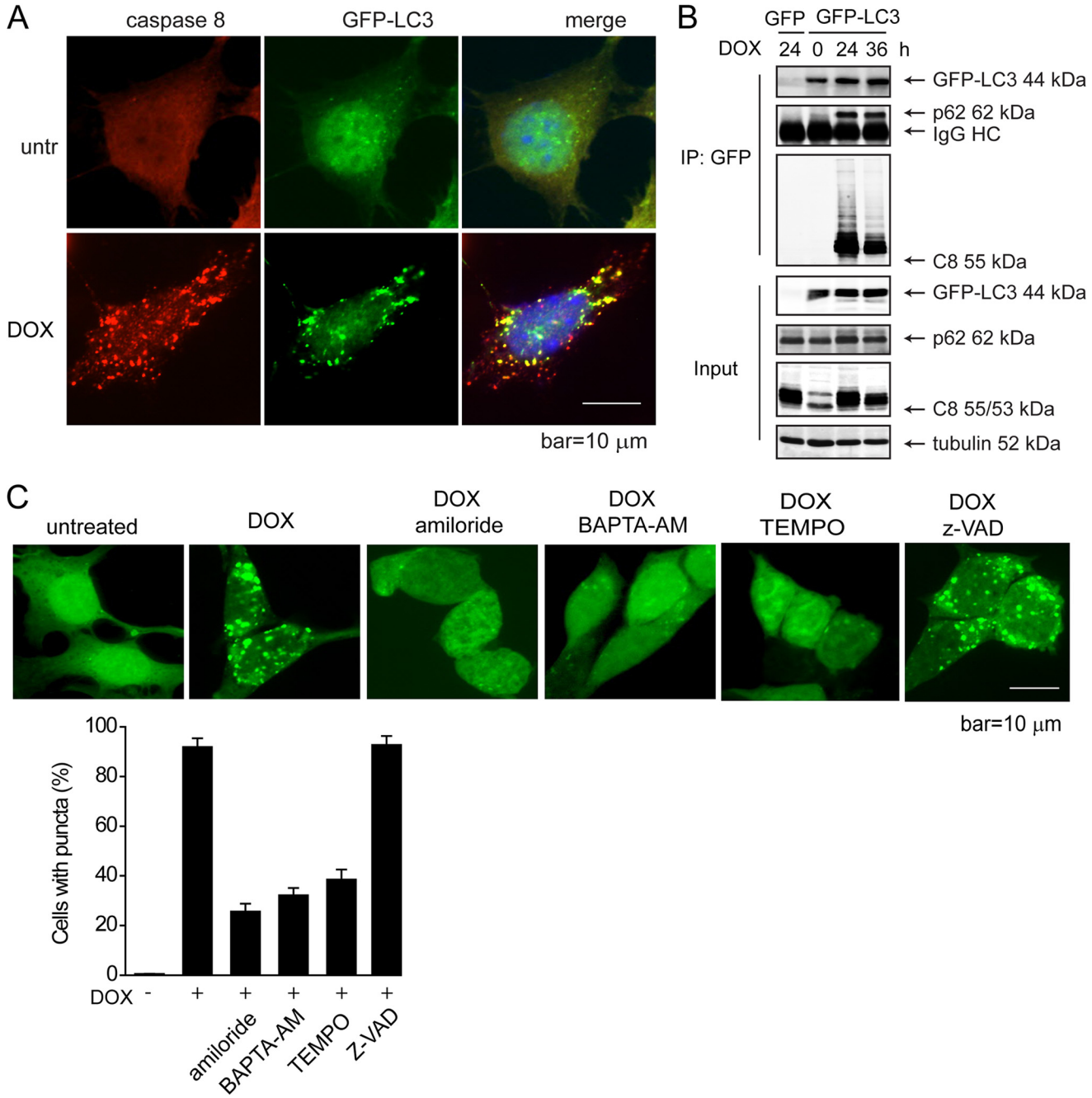


FIGURE 5. **MDEG G430F leads to increased protein aggregation and enhanced interaction of LC3, caspase-8, and p62.** *A*, MDEG G430F cells with the stable expression of GFP-LC3 were left untreated (*untr*) or treated with DOX. 24 h later, immunofluorescence was performed using an anti-caspase-8 antibody (*red*). DAPI was used to visualize the nucleus. Note the punctate distribution of GFP-LC3 and caspase-8 and their co-localization upon DOX treatment. *B*, MDEG G430F cells with the stable expression of GFP or GFP-LC3 were left untreated or treated with DOX for the indicated times. Cell lysates were subjected to immunoprecipitation (*IP*) with an anti-GFP antibody and probed for the indicated proteins. *C*, MDEG G430F cells with the stable expression of GFP-LC3 were left untreated or treated with DOX alone or together with amiloride, BAPTA-AM, TEMPOL, or z-VAD-fmk. 24 h later, cells were fixed and observed under a deconvolution fluorescence microscope. Representative images are shown. Quantification of cells with LC3 puncta was performed as described under "Experimental Procedures." Data shown are averages of five blind counts ± S.D.

punctate structures containing caspase-8 and GFP-LC3, which at least partially co-localized (Fig. 5*A*). Co-immunoprecipitation showed that MDEG G430F expression induced association of p62, LC3, and caspase-8 (Fig. 5*B*). These LC3-, p62-, and caspase-8-containing structures were reminiscent of the protein aggregates observed upon proteasome inhibition, which were distinct from starvation-induced autophagic puncta (24). The formation of the LC3-containing protein aggregates was blocked by amiloride, BAPTA-AM, and TEMPOL, but not by z-VAD-fmk (Fig. 5*C*). Together, these data indicate that the protein aggregation is mediated by proteasome inhibition downstream of MDEG hyperactivation-induced intracellular rise of calcium and ROS and is upstream of caspase activation.

*MDEG G430F-induced Apoptosis Is Dependent on LC3 and p62*—The above results indicate that MDEG G430F-induced cell death resembles the recently described caspase-8-mediated

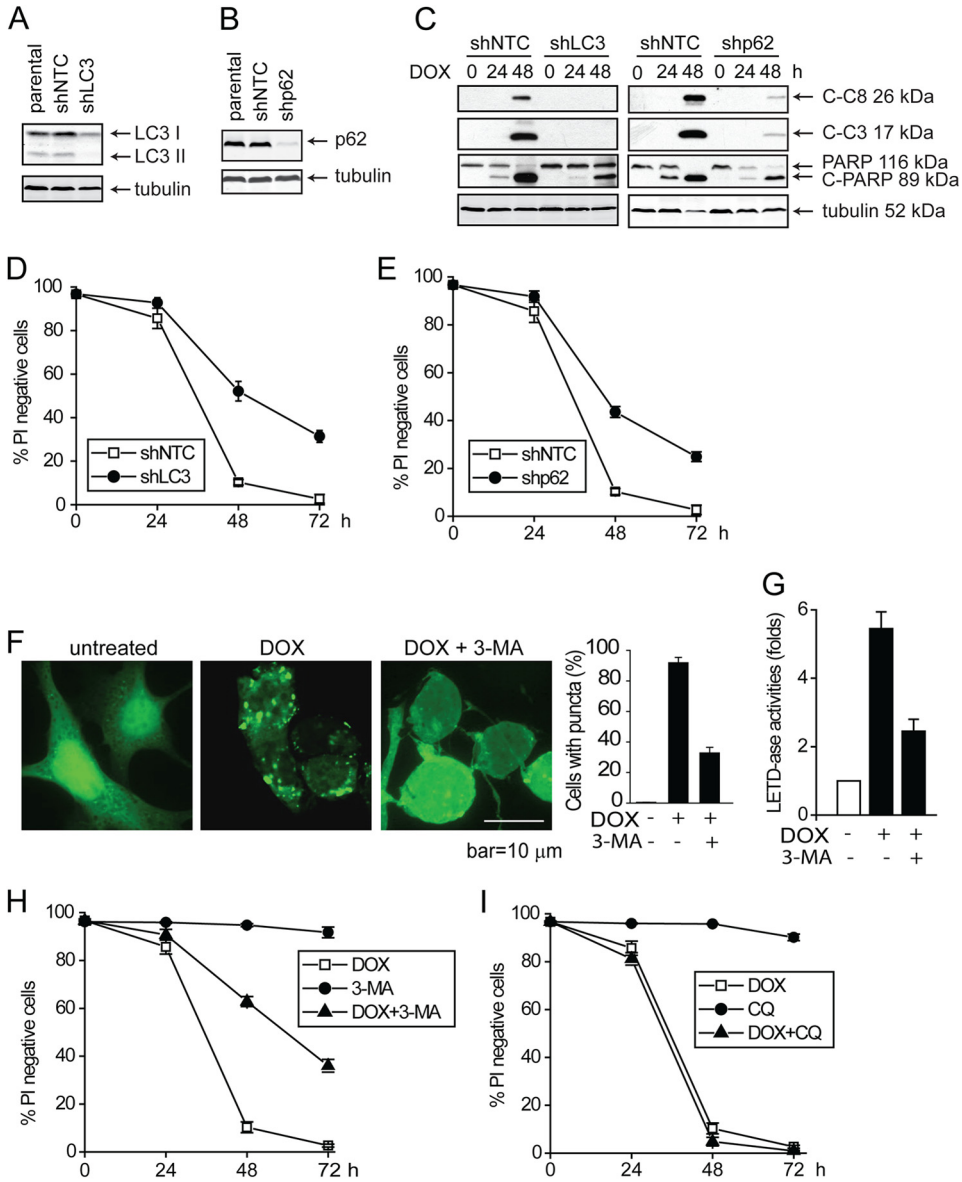


FIGURE 6. **MDEG G430F induces apoptosis in a p62- and LC3-dependent manner.** *A–E*, MDEG G430F cells were infected with lentiviral nontargeting control (*shNTC*) or shRNA against LC3 (*shLC3*) or p62 (*shp62*). Silencing of LC3 (*A*) and p62 (*B*) was verified by immunoblotting. *C*, MDEG G430F cells with stable shNTC, shLC3, and shp62 were treated with DOX. Cell lysates were examined by immunoblotting for the indicated proteins. *D* and *E*, cell death of MDEG G430F cells with the stable expression shLC3 (*D*) and shp62 (*E*) was measured by PI exclusion. The average of three independent assays ± S.D. is shown. *F*, MDEG G430F cells with stable expression of GFP-LC3 were left untreated or treated with DOX or DOX plus 3-MA. 24 h later, cells were observed under a deconvolution fluorescence microscope. The percentage of cells with more than 10 obvious puncta was obtained from five blind counts. Representative images are shown. *G* and *H*, MDEG G430F cells were treated with DOX alone or together with 3-MA. 24 h later, caspase-8 activity was measured (*G*), and cell death was measured by PI exclusion (*H*). The average of three independent assays ± S.D. is shown. *I*, MDEG G430F cells were cultured with DOX alone or together with chloroquine (*CQ*). Cell death was measured by PI exclusion. The average of three independent assays ± S.D. is shown.

apoptosis induced by proteasome inhibition, which is dependent on the autophagy-related proteins LC3 and p62 (24, 30). Therefore, we went on to determine whether MDEG G430F-induced apoptosis is also mediated by LC3 and p62. Silencing of LC3 or p62 by shRNA (Fig. 6, *A* and *B*) significantly blocked MDEG G430F-induced caspase activation (Fig. 6*C*) and cell death (Fig. 6, *D* and *E*). Moreover, 3-MA, a pharmacological inhibitor of phosphatidylinositol 3-kinase that has been shown to block LC3 lipidation and targeting to intracellular membranes, thereby blocking LC3 aggregation and apoptosis upon proteasome inhibition (24, 30), was tested for its effect on MDEG G430F-induced cell death. Indeed, 3-MA treatment blocked MDEG G430F-induced LC3 aggregation (Fig. 6*F*), caspase-8 activation (Fig. 6*G*), and cell death (Fig. 6*H*). In contrast, chloroquine, the lysosomal inhibitor that blocks autophagic degradation but not LC3 aggregation, did not inhibit apoptosis upon MDEG G430F expression (Fig. 6*I*). Taken together, these results indicate that MDEG G430F-induced cell death resembles that induced by proteasome inhibition, which is facilitated by LC3 and p62.

## DISCUSSION

In this study, we show that expression of the hyperactivation mutant of the ENaC channel, MDEG G430F, leads to intracel-

lular calcium rise, ROS generation, and proteasome and autophagy inhibition. This proteasome inhibition leads to an accumulation of polyubiquitinated proteins including caspase-8. Polyubiquitinated proteins are normally recognized by p62, and via its interaction with LC3, are delivered to the autophagosome for degradation. However, as autophagic degradation is blocked by MDEG G430F, the LC3- and p62-containing protein aggregates accumulate and facilitate caspase-8 oligomerization, activation, and apoptosis. According to this model, one would predict that silencing of p62 or LC3, or preventing of LC3 accumulation on autophagosome membranes, would lead to decreased protein aggregation and suppressed apoptosis. This is indeed the case as shRNA silencing of p62 or LC3, or inhibition of LC3 membrane localization by 3-MA, suppressed MDEG G430F-induced cell death (Fig. 6). The caspase-8 activation upon protein aggregation is consistent with the literature showing that expanded polyglutamine repeats induce a caspase-8-mediated cell death (33) and is reminiscent of recent studies including those of our own group showing that pharmacological or genetic inhibition of proteasomal and autophagolysosomal protein degradation pathways leads to caspase-8-mediated apoptosis (23, 24, 30). In addition, our results are consistent with a study in *C. elegans* showing that inactivation of unc-51, bec-1, and lgg-1, the worm counterparts of autophagy proteins Atg1, Atg6, and Atg8 (LC3), suppresses neural degeneration induced by hyperactivation mutants of MEC-4 and DEG-1 (34).

Our results show that MDEG G430F can cause intracellular $Ca^{2+}$ rise (Fig. 2, *A* and *B*), and that MDEG G430F-induced cell death can be blocked by BAPTA-AM (Fig. 2*C*). This is consistent with the hyperactivation mutant of the MEC-4 $Na^+$ channel MEC-4(d), which has been found to induce *C. elegans* neuronal cell death by promoting intracellular calcium rise (8). In *C. elegans*, MEC-4(d) induces $Ca^{2+}$ influx and promotes endoplasmic reticulum $Ca^{2+}$ release (8, 9). However, in mammalian cells, the DEG/ENaC members including MDEG G430F are $Ca^{2+}$-impermeable (7, 11, 35). Hence, the MDEG G430F-induced intracellular $Ca^{2+}$ increase is unlikely to be mediated by extracellular $Ca^{2+}$ entry; rather, it is likely to be mediated through endoplasmic reticulum $Ca^{2+}$ release provoked by excess $Na^+$ entry. This notion is supported by our observation that MDEG G430F-induced cell death was blocked by the cell-permeable $Ca^{2+}$ chelator BAPTA-AM (Fig. 2*C*), but not by the cell-impermeable chelators BAPTA and EGTA (Fig. 2*D*). The precise mechanism for MDEG G430F-induced intracellular $Ca^{2+}$ rise remains to be determined.

Our results also show that the increased redox stress plays a critical role in MDEG G430F-induced cell death. Increased ROS generation was observed upon MDEG G430F expression (Fig. 2*E*). This increased ROS is likely to be caused by the intracellular $Ca^{2+}$ rise as BAPTA-AM could inhibit the ROS increase in MDEG G430F-expressing cells (Fig. 2*E*). It is well documented that cytoplasmic $Ca^{2+}$ rise can lead to increased ROS production, most likely via mitochondrial $Ca^{2+}$ overload that stimulates mitochondrial metabolic activity (22). In agreement with the critical role of redox stress in MDEG G430F-induced cell death, ROS scavengers could block cell death (Fig. 2, *E* and *F*), as well as the upstream events including proteasome inhibition, protein aggregation, and caspase-8 activation upon MDEG G430F expression (Figs. 3, 4, and 5). To our knowledge, this is the first report of a link between redox stress and cell death induced by DEG/ENaC hyperactivation.

As both cytoplasmic $Ca^{2+}$ rise and ROS generation play critical roles in MDEG G430F-mediated cytotoxicity, our results further show that the cytotoxic effect is mediated by the inhibition of proteasomal and autophagolysosomal degradation pathways, which leads to the accumulation of caspase-8-containing protein aggregates and subsequent caspase-8 activation and apoptosis. Both cytosolic $Ca^{2+}$ rise and ROS elevation have been implicated in the regulation of protein quality control and degradation machineries. Cytosolic $Ca^{2+}$ levels are known to modulate proteasome activity (25, 26). Accumulation of oxidatively damaged proteins can lead to a reduction in proteasome activity (27). Although the role of $Ca^{2+}$ in regulating autophagy remains controversial (36–39), some recent studies suggest that $Ca^{2+}$ inhibits autophagy (40–43). The discrepancy could be due to the extent and duration of intracellular $Ca^{2+}$ increase as well as cell type specificity. Our current study shows that autophagy flux is inhibited by MDEG G430F expression (Fig. 4*C*). The inhibition of autophagy may be caused by intracellular $Ca^{2+}$ increase and/or through profound proteasomal inhibition that can lead to inhibition of autophagy possibly by "clogging" the autophagic degradation system (24, 31, 32). Nevertheless, our finding that inhibition of autophagy flux is involved in MDEG G430F-mediated cell death is consistent with the model that LC3 serves as a platform for the formation of protein aggregates that contain p62 and polyubiquitinated caspase-8 upon inhibition of protein degradation (23, 24, 30).

Our study provides a previously unknown mechanism for the cytotoxicity induced by hyperactivation of DEG/ENaC in mammalian cells, namely through a $Ca^{2+}$-mediated protein degradation inhibition and caspase-8 activation. This is different from the neural degeneration mediated by the activation of calpain proteases and aspartyl proteases upon the channel hyperactivation in *C. elegans*. Although we do not exclude the possibility that $Ca^{2+}$-dependent activation of lysosomal hydrolases may be involved in MDEG G430F-mediated cytotoxicity, our findings provide a novel mechanism that involves the activation of caspase-8. This will help with the understanding of ion channel hyperactivation-related pathological conditions and provide novel therapeutic strategies to target protein aggregation by silencing p62 and/or LC3 for DEG/ENaC-related diseases such as heart failure and stroke.

*Acknowledgment—We thank Dr. Michel Lazdunski (Institut de Pharmacologie Moleculaire et Cellulaire) for the MDEG wild-type and G430F expression constructs.*

## REFERENCES

1. Kellenberger, S., and Schild, L. (2002) Epithelial sodium channel/degenerin family of ion channels: a variety of functions for a shared structure. *Physiol. Rev.* **82,** 735–767
2. Qadri, Y. J., Rooj, A. K., and Fuller, C. M. (2012) ENaCs and ASICs as therapeutic targets. *Am. J. Physiol. Cell Physiol.* **302,** C943–965

3. Chu, X. P., Papasian, C. J., Wang, J. Q., and Xiong, Z. G. (2011) Modulation of acid-sensing ion channels: molecular mechanisms and therapeutic potential. *Int. J. Physiol. Pathophysiol. Pharmacol.* **3,** 288–309
4. Li, M., and Xiong, Z. G. (2011) Ion channels as targets for cancer therapy. *Int. J. Physiol. Pathophysiol. Pharmacol.* **3,** 156–166
5. Chalfie, M., and Wolinsky, E. (1990) The identification and suppression of inherited neurodegeneration in *Caenorhabditis elegans*. *Nature* **345,** 410–416
6. Driscoll, M., and Chalfie, M. (1991) The *mec-4* gene is a member of a family of *Caenorhabditis elegans* genes that can mutate to induce neuronal degeneration. *Nature* **349,** 588–593
7. Bassilana, F., Champigny, G., Waldmann, R., de Weille, J. R., Heurteaux, C., and Lazdunski, M. (1997) The acid-sensitive ionic channel subunit ASIC and the mammalian degenerin MDEG form a heteromultimeric $H^+$-gated $Na^+$ channel with novel properties. *J. Biol. Chem.* **272,** 28819–28822
8. Bianchi, L., Gerstbrein, B., Frøkjaer-Jensen, C., Royal, D. C., Mukherjee, G., Royal, M. A., Xue, J., Schafer, W. R., and Driscoll, M. (2004) The neurotoxic MEC-4(d) DEG/ENaC sodium channel conducts calcium: implications for necrosis initiation. *Nat. Neurosci.* **7,** 1337–1344
9. Xu, K., Tavernarakis, N., and Driscoll, M. (2001) Necrotic cell death in *C. elegans* requires the function of calreticulin and regulators of $Ca^{2+}$ release from the endoplasmic reticulum. *Neuron* **31,** 957–971
10. Syntichaki, P., Xu, K., Driscoll, M., and Tavernarakis, N. (2002) Specific aspartyl and calpain proteases are required for neurodegeneration in *C. elegans*. *Nature* **419,** 939–944
11. Waldmann, R., Champigny, G., Voilley, N., Lauritzen, I., and Lazdunski, M. (1996) The mammalian degenerin MDEG, an amiloride-sensitive cation channel activated by mutations causing neurodegeneration in *Caenorhabditis elegans*. *J. Biol. Chem.* **271,** 10433–10436
12. Ausserlechner, M. J., Obexer, P., Deutschmann, A., Geiger, K., and Kofler, R. (2006) A retroviral expression system based on tetracycline-regulated tricistronic transactivator/repressor vectors for functional analyses of antiproliferative and toxic genes. *Mol. Cancer Ther.* **5,** 1927–1934
13. Ullman, E., Fan, Y., Stawowczyk, M., Chen, H. M., Yue, Z., and Zong, W. X. (2008) Autophagy promotes necrosis in apoptosis-deficient cells in response to ER stress. *Cell Death Differ.* **15,** 422–425
14. Luker, G. D., Pica, C. M., Song, J., Luker, K. E., and Piwnica-Worms, D. (2003) Imaging 26S proteasome activity and inhibition in living mice. *Nat. Med.* **9,** 969–973
15. Madesh, M., Hawkins, B. J., Milovanova, T., Bhanumathy, C. D., Joseph, S. K., Ramachandrarao, S. P., Sharma, K., Kurosaki, T., and Fisher, A. B. (2005) Selective role for superoxide in $InsP_3$ receptor-mediated mitochondrial dysfunction and endothelial apoptosis. *J. Cell Biol.* **170,** 1079–1090
16. Dou, Z., Chattopadhyay, M., Pan, J. A., Guerriero, J. L., Jiang, Y. P., Ballou, L. M., Yue, Z., Lin, R. Z., and Zong, W. X. (2010) The class IA phosphatidylinositol 3-kinase p110-$\beta$ subunit is a positive regulator of autophagy. *J. Cell Biol.* **191,** 827–843
17. Chung, S., Gumienny, T. L., Hengartner, M. O., and Driscoll, M. (2000) A common set of engulfment genes mediates removal of both apoptotic and necrotic cell corpses in *C. elegans*. *Nat. Cell Biol.* **2,** 931–937
18. Degenhardt, K., Sundararajan, R., Lindsten, T., Thompson, C., and White, E. (2002) Bax and Bak independently promote cytochrome *c* release from mitochondria. *J. Biol. Chem.* **277,** 14127–14134
19. Wei, M. C., Lindsten, T., Mootha, V. K., Weiler, S., Gross, A., Ashiya, M., Thompson, C. B., and Korsmeyer, S. J. (2000) tBID, a membrane-targeted death ligand, oligomerizes BAK to release cytochrome *c*. *Genes Dev.* **14,** 2060–2071
20. Zong, W. X., Lindsten, T., Ross, A. J., MacGregor, G. R., and Thompson, C. B. (2001) BH3-only proteins that bind pro-survival Bcl-2 family members fail to induce apoptosis in the absence of Bax and Bak. *Genes Dev.* **15,** 1481–1486
21. Cheng, E. H., Wei, M. C., Weiler, S., Flavell, R. A., Mak, T. W., Lindsten, T., and Korsmeyer, S. J. (2001) BCL-2, BCL-$X_L$ sequester BH3 domain-only molecules preventing BAX- and BAK-mediated mitochondrial apoptosis. *Mol. Cell* **8,** 705–711
22. Mallilankaraman, K., Doonan, P., Cárdenas, C., Chandramoorthy, H. C., Müller, M., Miller, R., Hoffman, N. E., Gandhirajan, R. K., Molgó, J., Birnbaum, M. J., Rothberg, B. S., Mak, D. O., Foskett, J. K., and Madesh, M. (2012) MICU1 is an essential gatekeeper for MCU-mediated mitochondrial $Ca^{2+}$ uptake that regulates cell survival. *Cell* **151,** 630–644
23. Ullman, E., Pan, J. A., and Zong, W. X. (2011) Squamous cell carcinoma antigen 1 promotes caspase-8-mediated apoptosis in response to endoplasmic reticulum stress while inhibiting necrosis induced by lysosomal injury. *Mol. Cell. Biol.* **31,** 2902–2919
24. Pan, J. A., Ullman, E., Dou, Z., and Zong, W. X. (2011) Inhibition of protein degradation induces apoptosis through a microtubule-associated protein 1 light chain 3-mediated activation of caspase-8 at intracellular membranes. *Mol. Cell. Biol.* **31,** 3158–3170
25. Kawahara, H., and Yokosawa, H. (1994) Intracellular calcium mobilization regulates the activity of 26 S proteasome during the metaphase-anaphase transition in the ascidian meiotic cell cycle. *Dev. Biol.* **166,** 623–633
26. Voges, D., Zwickl, P., and Baumeister, W. (1999) The 26S proteasome: a molecular machine designed for controlled proteolysis. *Annu. Rev. Biochem.* **68,** 1015–1068
27. Conconi, M., Szweda, L. I., Levine, R. L., Stadtman, E. R., and Friguet, B. (1996) Age-related decline of rat liver multicatalytic proteinase activity and protection from oxidative inactivation by heat-shock protein 90. *Arch. Biochem. Biophys.* **331,** 232–240
28. Ding, W. X., Ni, H. M., Gao, W., Yoshimori, T., Stolz, D. B., Ron, D., and Yin, X. M. (2007) Linking of autophagy to ubiquitin-proteasome system is important for the regulation of endoplasmic reticulum stress and cell viability. *Am. J. Pathol.* **171,** 513–524
29. Korolchuk, V. I., Menzies, F. M., and Rubinsztein, D. C. (2010) Mechanisms of cross-talk between the ubiquitin-proteasome and autophagy-lysosome systems. *FEBS Lett.* **584,** 1393–1398
30. Young, M. M., Takahashi, Y., Khan, O., Park, S., Hori, T., Yun, J., Sharma, A. K., Amin, S., Hu, C. D., Zhang, J., Kester, M., and Wang, H. G. (2012) Autophagosomal membrane serves as platform for intracellular death-inducing signaling complex (iDISC)-mediated caspase-8 activation and apoptosis. *J. Biol. Chem.* **287,** 12455–12468
31. Ding, W. X., and Yin, X. M. (2008) Sorting, recognition and activation of the misfolded protein degradation pathways through macroautophagy and the proteasome. *Autophagy* **4,** 141–150
32. Korolchuk, V. I., Mansilla, A., Menzies, F. M., and Rubinsztein, D. C. (2009) Autophagy inhibition compromises degradation of ubiquitin-proteasome pathway substrates. *Mol. Cell* **33,** 517–527
33. Sánchez, I., Xu, C. J., Juo, P., Kakizaka, A., Blenis, J., and Yuan, J. (1999) Caspase-8 is required for cell death induced by expanded polyglutamine repeats. *Neuron* **22,** 623–633
34. Tóth, M. L., Simon, P., Kovács, A. L., and Vellai, T. (2007) Influence of autophagy genes on ion-channel-dependent neuronal degeneration in *Caenorhabditis elegans*. *J. Cell Sci.* **120,** 1134–1141
35. Kellenberger, S., Hoffmann-Pochon, N., Gautschi, I., Schneeberger, E., and Schild, L. (1999) On the molecular basis of ion permeation in the epithelial $Na^+$ channel. *J. Gen. Physiol.* **114,** 13–30
36. Høyer-Hansen, M., Bastholm, L., Szyniarowski, P., Campanella, M., Szabadkai, G., Farkas, T., Bianchi, K., Fehrenbacher, N., Elling, F., Rizzuto, R., Mathiasen, I. S., and Jäättelä, M. (2007) Control of macroautophagy by calcium, calmodulin-dependent kinase kinase-$\beta$, and Bcl-2. *Mol. Cell* **25,** 193–205
37. Sakaki, K., Wu, J., and Kaufman, R. J. (2008) Protein kinase C$\theta$ is required for autophagy in response to stress in the endoplasmic reticulum. *J. Biol. Chem.* **283,** 15370–15380
38. Gao, W., Ding, W. X., Stolz, D. B., and Yin, X. M. (2008) Induction of macroautophagy by exogenously introduced calcium. *Autophagy* **4,** 754–761
39. Lam, D., Kosta, A., Luciani, M. F., and Golstein, P. (2008) The inositol 1,4,5-trisphosphate receptor is required to signal autophagic cell death. *Mol. Biol. Cell* **19,** 691–700
40. Sarkar, S., Floto, R. A., Berger, Z., Imarisio, S., Cordenier, A., Pasco, M., Cook, L. J., and Rubinsztein, D. C. (2005) Lithium induces autophagy by inhibiting inositol monophosphatase. *J. Cell Biol.* **170,** 1101–1111
41. Criollo, A., Maiuri, M. C., Tasdemir, E., Vitale, I., Fiebig, A. A., Andrews, D., Molgó, J., Díaz, J., Lavandero, S., Harper, F., Pierron, G., di Stefano, D.,

Rizzuto, R., Szabadkai, G., and Kroemer, G. (2007) Regulation of autophagy by the inositol trisphosphate receptor. *Cell Death Differ.* **14,** 1029–1039

42. Cárdenas, C., Miller, R. A., Smith, I., Bui, T., Molgó, J., Müller, M., Vais, H., Cheung, K. H., Yang, J., Parker, I., Thompson, C. B., Birnbaum, M. J., Hallows, K. R., and Foskett, J. K. (2010) Essential regulation of cell bioenergetics by constitutive $InsP_3$ receptor $Ca^{2+}$ transfer to mitochondria. *Cell* **142,** 270–283
43. Harr, M. W., McColl, K. S., Zhong, F., Molitoris, J. K., and Distelhorst, C. W. (2010) Glucocorticoids down-regulate Fyn and inhibit $IP_3$-mediated calcium signaling to promote autophagy in T lymphocytes. *Autophagy* **6,** 912–921